Mechanical Systems and Signal Processing 90 (2017) 126–140

Contents lists available at ScienceDirect

Mechanical Systems and Signal Processing

journal homepage: www.elsevier.com/locate/ymssp

Theoretical and experimental investigation into structural and fluid motions at low frequencies in water distribution pipes

Yan Gao [a,*], Yuyou Liu [b,c]

[a] Key Laboratory of Noise and Vibration Research, Institute of Acoustics, Chinese Academy of Sciences, Beijing 100190, China
[b] Beijing Municipal Institute of Labour Protection, Beijing 100054, China
[c] Environment & Ground Engineering, UK & Ireland, AECOM, London SW19 4DR, UK

ARTICLE INFO

Article history:
Received 16 June 2016
Received in revised form 10 December 2016
Accepted 14 December 2016
Available online 28 December 2016

Keywords:
Water distribution pipe
Pipe wall displacement
Internal pressure
Axisymmetric wave
Sensor

ABSTRACT

Vibrational energy is transmitted in buried fluid-filled pipes in a variety of wave types. Axisymmetric ($n = 0$) waves are of practical interest in the application of acoustic techniques for the detection of leaks in underground pipelines. At low frequencies $n = 0$ waves propagate longitudinally as fluid-dominated ($s = 1$) and shell-dominated ($s = 2$) waves. Whilst sensors such as hydrophones and accelerometers are commonly used to detect leaks in water distribution pipes, the mechanism governing the structural and fluid motions is not well documented. In this paper, the low-frequency behaviour of the pipe wall and the contained fluid is investigated. For most practical pipework systems, these two waves are strongly coupled; in this circumstance the ratios of the radial pipe wall displacements along with the internal pressures associated with these two wave types are obtained.

Numerical examples show the relative insensitivity of the structural and fluid motions to the $s = 2$ wave for both metallic and plastic pipes buried in two typical soils. It is also demonstrated that although both acoustic and vibration sensors at the same location provide the identical phase information of the transmitted signals, pressure responses have significantly higher levels than acceleration responses, and thus hydrophones are better suited in a low signal-to-noise ratio (SNR) environment. This is supported by experimental work carried out at a leak detection facility. Additional pressure measurements involved excitation of the fluid and the pipe fitting (hydrant) on a dedicated water pipe. This work demonstrates that the $s = 1$ wave is mainly responsible for the structural and fluid motions at low frequencies in water distribution pipes as a result of water leakage and direct pipe excitation.

1. Introduction

Pipelines are the most economic and safest mode of transportation for fluid and gases in a wide range of practical engineering environments. Whilst they are designed and constructed to fulfill high demands of safety and reliability, it is difficult to avoid the occurrence of leakage resulting from sudden changes in pressure, corrosion, cracks, material defects, ground movement due to seasonal changes, or even poor workmanship. Pipeline leakage has been a major concern due to the

* Corresponding author.
E-mail address: gaoyan@mail.ioa.ac.cn (Y. Gao).

http://dx.doi.org/10.1016/j.ymssp.2016.12.018
0888-3270/

significant environmental damage and economic losses. For example, every day, huge amount of clean, treated water is lost through leakage from water supply networks [1,2]; explosions caused by leaking oil and gases from underground piping systems have frequently made headlines in recent years. A variety of techniques have been developed for the detection and location of pipeline leakage in recent years [3–7]. Up to date, there is not yet an approach that can efficiently detect leaks in any of these pipe systems.

Acoustic techniques have proven to be effective and are widely used to locate leaks in water distribution pipes in many years [8–11]. It is believed that leak noise is concentrated at low frequencies, in particular in plastic water distribution pipes [12–16], although acoustic emission sensors have been attempted to acquire high-frequency leak signals up to 100–300 kHz [17,18]. In general, the upper frequency limit of measured leak noise is found to be 1 kHz for metal pipes and only 200 Hz for plastic pipes. Other non-acoustic techniques, such as hydraulic methods [19], ground-penetrating radar, tracer gas and magnetic fields [20] have also been investigated for the application of water leak detection.

For acoustic leak detection techniques, most of the methods and equipments proposed are based on the vibro-acoustic measurements in water distribution pipes. Water escaping from pressurised pipes generates leak noise that travels by two roots, including through the soil to the ground surface, and in the pipe wall and the water. Correspondingly, practice leak detection surveys are commonly performed by utilizing equipments based on vibro-acoustic sensors, such as listening devices above ground, namely geophones and listening rods, and hydrophones or accelerometers at two access points such as hydrants and valves. With the latter, leak signals are then transmitted to the leak noise correlator to pinpoint a suspected leak. Acoustic methods based on cross-correlation provide a powerful solution for locating leaks, even where there is substantial background noise or only the quietest of leak noise is present.

Leak noise travels in both directions away from the leak through the pipe wall (as minute vibrations) and through the water column (as a pressure wave). In the "classic" correlation process, two accelerometers are attached magnetically to access points on pipe fittings (i.e., "dry" connection) bridging the suspected leak on the water main. In difficult situations such as for the pipe being plastic, with large diameter and large burial depth, "wet" connection may be adopted (optionally) using hydrophones connected to hydrants. For these methods to be effective, the propagation wavespeed need to be know *a priori*. Plastic pipes have proven to be problematic due to the uncertainty in the propagation wavespeed and large wave attenuation. Previous work by Gao et al. [12–14] has shown that the cross-correlation methods are most successfully conducted on low frequency leak signals resulting from an approximately non-dispersive propagating wave.

The way in which vibration and waves propagate in fluid-filled pipes *in vacuo* has been discussed previously [21–23]. Fuller and Fahy [21] derived the wavenumbers for fluid-filled pipes defined as "hard" and "soft" shells. Fuller [22] further investigated theoretically the energy distribution among various wave types for a radial wall input force and for internal pressure pulsations. Pinnington and Briscoe [23] introduced an external circumferential piezoelectric transducer to detect the radial wall motion of a fluid-filled pipe. It has been shown for a multiple jointed pipe system with fluid and pipe wall excitations, two axisymmetric ($n = 0$) wave types are excited, including a predominantly fluid-dominated ($s = 1$) wave and a predominantly shell-dominated ($s = 2$) wave. These two waves are primarily longitudinal involving both structural and fluid motions, and the strength of coupling between these motions is governed by the pipe's dimensions and physical properties. The $s = 1$ wave is predominantly fluid-based with some radial shell motion associated with the shell compliance, and the $s = 2$ wave is predominantly a compressional wave in the shell with some associated radial wall motion influenced by Poisson's ratio and fluid loading. Since the $s = 1, 2$ waves are strongly coupled, even pure pressure or pipe wall excitations will lead to both structure and fluid motions.

Substantial research [23–26] has involved modelling of the $s = 1, 2$ wavenumbers, together with experimental investigations of the $s = 1$ wave that propagates in a fluid-filled pipe. Pinnington and Briscoe [23] first derived the analytical solutions to the wavenumbers for a fluid-filled pipe *in vacuo* and calculated the relative sizes of the two wave types for various boundary conditions in soft and hard-walled pipes. Muggleton *et al.* [24] derived the wavenumber expressions for a buried fluid-filled pipe under lubricated contact, in which the frictional stress is presumed to be zero at the pipe-soil interface. For leak detection in buried pipes, however, the relative motion of the pipe and soil is unlikely to occur. Therefore, the pipe is more appropriate to be assumed to be in perfect contact with the surrounding soil, for which displacement continuity conditions are fully satisfied. Gao *et al.* [25] have recently developed an analytical method for investigating the coupled equations of $n = 0$ motion in a buried fluid-filled pipe. Furthermore, an expression for the $s = 1$ wavenumber has been found and validated by some wavenumber measurements made on a buried MDPE water pipe [26].

Although it is believed that the $s = 1$ wave carries most of the acoustic energy at low frequencies in water distribution pipes, the contributions associated with the two wave types have not been well documented. A comprehensive analysis of the fully coupled system would be extremely complex and beyond the scope of the present paper. An approximate method is now adopted to quantify the contributions of the $s = 1, 2$ waves to the internal pressure and the radial pipe wall displacement, which is a similar approach to that taken by Pinnington and Briscoe [23]. This enables better understanding of the transducer sensitivities to these two waves. It builds on the coupled equations of motion given recently by the authors [25], which are solved for $s = 1, 2$ wavenumbers. Here, the results for the $s = 1$ wave are reproduced briefly for completeness. Ratios of the pipe wall displacements along with the internal pressures associated with these two waves are subsequently derived. Numerical analysis is then performed for both a metal and plastic water pipes. To support the theoretical analysis, measurements made from two buried water pipe systems are presented.

2. Theory of axisymmetric wave propagation

Consider the coupled axial and radial motion of a buried fluid-filled pipe with a mean radius a and wall thickness h such that $h/a \ll 1$. Referring to Fig. 1, u and w denote the displacements of the shell element in the x and r directions, respectively. The internal fluid is assumed to be inviscid and the surrounding soil is assumed to be elastic, homogenous and isotropic. Losses within the fluid and surrounding soil are neglected. Coupled equations of motion for the $n = 0$ waves that propagate in a buried fluid-filled pipe have been derived in recent work [25]. In the analysis, the pipe is assumed to be in perfect contact with the surrounding soil such that no slippage occurs at the pipe-soil interface. Here travelling wave solutions of the form $u = \sum_{s=1}^{2} U_s e^{i(\omega t - k_s x)}$, $w = \sum_{s=1}^{2} W_s e^{i(\omega t - k_s x)}$ and $p_f = \sum_{s=1}^{2} P_{fs} J_0(k_{fs}^r r) e^{i(\omega t - k_s x)}$ are used to describe the pipe wall displacements and internal pressure, where k_s is the axial wavenumber for the two wave types $s = 1, 2$; U_s and W_s are the amplitudes of shell displacements in the axial and radial directions respectively; P_{fs} is the amplitude of the internal pressure; $J_0()$ represents a Bessel function of order zero; the internal fluid radial wavenumber, k_{fs}^r, is related to the free-field fluid wavenumber, k_f, by $(k_{fs}^r)^2 = k_f^2 - k_s^2$ and $k_f^2 = \omega^2 \rho_f / B_f$; B_f and ρ_f are the bulk modulus and density of the internal fluid; and ω is the angular frequency.

Consider the equations governing the coupled axial and radial motion for the axisymmetric s waves in a buried fluid-filled pipe [25]

$$\begin{bmatrix} \Omega^2 - (k_s a)^2 - SL_{11} & -i\upsilon_p (k_s a) - SL_{12} \\ -i\upsilon_p (k_s a) - SL_{21} & 1 - \Omega^2 - FL - SL_{22} \end{bmatrix} \begin{bmatrix} U_s \\ W_s \end{bmatrix} = \mathbf{0} \tag{1}$$

where Ω is the nondimensional frequency, $\Omega = k_L a$; k_L is the shell compressional wavenumber, $k_L^2 = \omega^2 \rho_p (1 - \upsilon_p^2)/E_p$; ρ_p, E_p and υ_p are the density, Young's modulus and Poisson's ratio of the shell; FL and $\mathbf{SL}$ are the fluid loading term and the soil loading matrix representing the coupling effects of the fluid and soil on the pipe wall respectively, and at low frequencies are given by [25]

$$FL = -2 \frac{\rho_f}{\rho_p} \frac{a}{h} \frac{\Omega^2}{k_f^2 a^2 - k_s^2 a^2} \tag{2}$$

The soil loading matrix, $\mathbf{SL}$, is given by [25]

$$\left.\begin{aligned} SL_{11} &= -\mu_m \frac{(1-\upsilon_p^2)}{E_p} \frac{a}{h} \frac{k_{ds}^r a k_r^2 a^2}{k_{rs}^r a k_{ds}^r a [H_0(k_{rs}^r a)/H_0'(k_{rs}^r a)] + k_s^2 a^2 [H_0(k_{ds}^r a)/H_0'(k_{ds}^r a)]} \\ SL_{12} &= i\mu_m \frac{(1-\upsilon_p^2)}{E_p} \frac{a}{h} k_s a \left\{ 2 - \frac{k_r^2 a^2 H_0(k_{ds}^r a)/H_0'(k_{ds}^r a)}{k_{rs}^r a k_{ds}^r a [H_0(k_{rs}^r a)/H_0'(k_{rs}^r a)] + k_s^2 a^2 [H_0(k_{ds}^r a)/H_0'(k_{ds}^r a)]} \right\} \\ SL_{21} &= SL_{12} \\ SL_{22} &= -\mu_m \frac{(1-\upsilon_p^2)}{E_p} \frac{a}{h} \left\{ 2 + \frac{k_{rs}^r a k_r^2 a^2 [H_0(k_{rs}^r a)/H_0'(k_{rs}^r a)][H_0(k_{ds}^r a)/H_0'(k_{ds}^r a)]}{k_{rs}^r a k_{ds}^r a [H_0(k_{rs}^r a)/H_0'(k_{rs}^r a)] + k_s^2 a^2 [H_0(k_{ds}^r a)/H_0'(k_{ds}^r a)]} \right\} \end{aligned}\right\} \tag{3a-d}$$

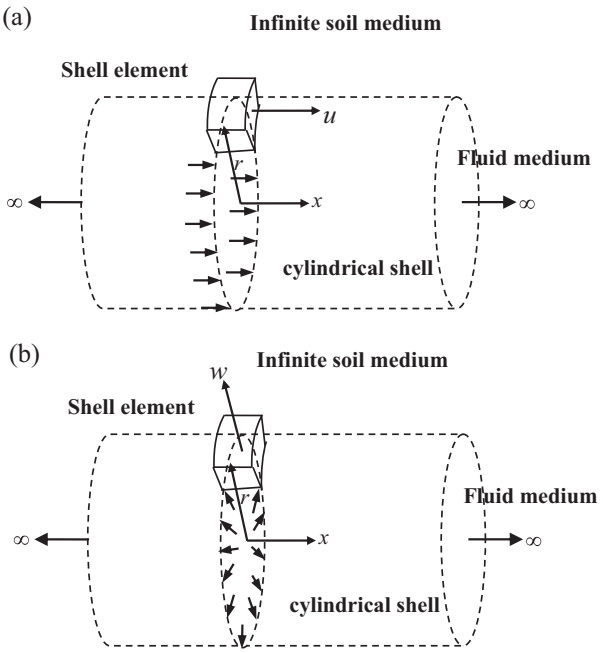

Fig. 1. Schematic of the coupled axial and radial motion of the shell element in cylindrical coordinates: (a) in the axial direction; (b) in the radial direction.

where the radial wavenumbers, k_{ds}^r and k_{rs}^r, are related to the compressional and shear wavenumbers in the surrounding medium, k_d and k_r, by $(k_{ds}^r)^2 = k_d^2 - k_s^2$ and $(k_{rs}^r)^2 = k_r^2 - k_s^2$ respectively; $k_d^2 = \omega^2\rho_m/(\lambda_m + 2\mu_m)$ and $k_r^2 = \omega^2\rho_m/\mu_m$; ρ_m, λ_m and μ_m are the density and Lamé coefficients of the surrounding soil; the Hankel functions of the second kind and zero order, $H_0()$, describe outgoing waves in the surrounding soil; and $H_0' = (\partial/\partial r)H_0()$.

The non-trivial solutions to the $s = 1, 2$ wavenumbers can be obtained by making the determinant of the characteristic matrix **L** given by Eq. (1) equal to zero, i.e., $\det[\mathbf{L}(k_s^2)] = 0$. This leads to the characteristic equation which describes the propagation of the s waves by

$$[\Omega^2 - (k_s a)^2 - SL_{11}][1 - \Omega^2 - FL - SL_{22}] - [\mathrm{i}\upsilon_p(k_s a) + SL_{12}]^2 = 0 \tag{4}$$

Since the soil loading matrix **SL** is a function of the wavenumber k_s, Eq. (4) is more amenable to calculation in a recursive manner. Based on the knowledge of the properties of the $s = 1, 2$ waves [23], the expressions for the $s = 1, 2$ wavenumbers can be derived to reduce the computational cost as follows,

2.1. The s = 1 wavenumber

For the $s = 1$ wave, it is noted that k_1 is much larger than the shell compressional wavenumber k_L. This means that the $s = 1$ wave travels much slower than the shell compressional wave. Therefore, assuming $k_1^2 a^2 \gg \Omega^2$, the characteristic equation given by Eq. (4) becomes

$$1 - \Omega^2 - FL - SL_{22} - \frac{(\upsilon_p - \mathrm{i}SL_{12}/k_1 a)^2}{1 + SL_{11}/k_1^2 a^2} = 0 \tag{5}$$

Substitution of the fluid loading term FL given by Eq. (2), Eq. (5) can be rearranged to give

$$k_1^2 = k_f^2\left(1 + \frac{\beta}{1 - \Omega^2 + \alpha}\right) \tag{6}$$

where α and β are the measures of the effects of soil and fluid loading on the pipe wall, and given by $\alpha = -SL_{22} - (\upsilon_p - \mathrm{i}SL_{12}/k_1 a)^2/(1 + SL_{11}/k_1^2 a^2)$, $\beta = 2B_f a(1 - \upsilon_p^2)/E_p h$.

2.2. The s = 2 wavenumber

The approximate solution for the $s = 2$ wavenumber, is obtained with the knowledge that k_2 is always smaller than the free-field fluid wavenumber k_f. This means that the $s = 2$ wavespeed is much faster than the free-field fluid wavespeed. Assuming $k_2^2 a^2 \ll k_f^2 a^2$, the fluid loading term FL given by Eq. (2) reduces to

$$FL = -\beta \tag{7}$$

Substituting Eqs. (7) into (4) gives the simplified characteristic equation which describes the propagation of the $s = 2$ wave by

$$\Omega^2 - (k_2 a)^2 - SL_{11} + (k_2 a)^2\frac{(\upsilon_p - \mathrm{i}SL_{12}/k_2 a)^2}{1 - \Omega^2 + \beta - SL_{22}} = 0 \tag{8}$$

Rearranging the above equation gives the $s = 2$ wavenumber by

$$k_2^2 = k_L^2\frac{1 - SL_{11}/\Omega^2}{1 - (\upsilon_p - \mathrm{i}SL_{12}/k_2 a)^2/(1 - \Omega^2 + \beta - SL_{22})} \tag{9}$$

3. Structural and fluid motions

This section starts with the relationships between the pipe wall motion and the fluid motion for each of the $s = 1, 2$ wave types. For most practical water distribution networks two waves are strongly coupled. In this circumstance the ratios of the radial pipe wall displacements and the internal pressures associated with these two waves are subsequently derived.

3.1. Relationships between the internal pressure and the pipe wall displacements

At the pipe-internal fluid interface $r = a$, each of the $s = 1, 2$ pressure waves in the contained fluid must have a radial displacement which is equal to the shell displacement. Equating the radial velocity of the fluid, given by the momentum equation, to that of the shell wall gives [21]

$$P_{fs} = \frac{\omega^2 \rho_f}{k_{fs}^r} \frac{1}{\mathrm{J}_0'(k_{fs}^r a)} W_s \tag{10}$$

where $\mathrm{J}_0' = (\partial/\partial r)\mathrm{J}_0()$. Adopt the low frequency approximation for the Bessel function, $\mathrm{J}_0'(k_{fs}^r a) \approx -k_{fs}^r a/2$ [27]. This suggests that at low frequencies, when there is less than one half of a fluid wavelength across the pipe diameter, the pressure is distributed uniformly across the section of the pipe. Therefore, the amplitude of the radial displacement of the pipe wall, W_s, is found to be

$$W_s = \chi_s P_{fs} \tag{11}$$

where $\chi_s = -(1 - k_s^2/k_f^2)/(2B_f/a)$. The relationship between the axial and radial displacements of the pipe wall can be obtained from Eq. (1), and is given by

$$U_s = \gamma_s W_s \tag{12}$$

where $\gamma_s = (1 - \Omega^2 - FL - SL_{22})/[\mathrm{i}\nu_p(k_s a) + SL_{21}]$.

3.2. Ratios of the radial pipe wall displacements and the internal pressures

The energies for the $s = 1, 2$ waves per unit pipe length, ε_1 and ε_2, are approximated by [23]

$$\varepsilon_1 \approx \frac{\pi a^2}{\rho_f c_1^2} \tilde{P}_{f1}^2; \quad \varepsilon_2 \approx 2\pi a h \rho_p \omega^2 \tilde{U}_2^2 \tag{13a, b}$$

where $\tilde{P}_{f1}^2$ and $\tilde{U}_2^2$ are the spatially averaged mean-square pressure and axial pipe wall displacement respectively. Here the internal pressure and the axial pipe wall displacement are related to the radial pipe wall displacement by Eqs. (11) and (12) respectively. For strong coupling, the energies are equipartitioned between the two waves, i.e.,

$$\varepsilon_1 c_1 = \varepsilon_2 c_2 \tag{14}$$

where c_1 and c_2 are the propagation wavespeeds for the $s = 1, 2$ waves respectively. Substituting Eqs. (13) into (14), after some manipulation, leads to the ratio of radial pipe wall displacements at low frequencies as

$$\left|\frac{W_2}{W_1}\right|^2 = \frac{aRe(k_1)Re(k_2)}{2h\rho_p\rho_f\omega^4|\chi_1\gamma_2|^2} \tag{15}$$

Furthermore, substituting Eqs. (11) into (15) leads to the relative ratio of the pressure amplitudes for the $s = 1, 2$ waves by

$$\left|\frac{P_{f2}}{P_{f1}}\right|^2 = \frac{aRe(k_1)Re(k_2)}{2h\rho_p\rho_f\omega^4|\chi_2\gamma_2|^2} \tag{16}$$

4. Numerical results

Numerical results are presented for a typical cast iron and a PVC water pipe buried in two soil types, representing a sandy soil and a clay soil, respectively. The relevant material properties assumed are given in Table 1, which provide consistency with the recent study carried out in [25]. The surrounding medium is assumed to be lossless. The complex wavenumbers for the $s = 1, 2$ waves are obtained using recursive algorithms at low frequencies up to 1 kHz, the real and imaginary parts of which give the wavespeeds and attenuations of the propagation waves respectively. The dispersion curves are plotted in Fig. 2. The calculated wavespeeds c_1 and c_2 are normalised with respect to the free-field wavespeed, c_f, and the shell compressional wavspeed, c_l, respectively; and the attenuations are defined by the loss in dB per unit propagation distance (measured in pipe radii).

Table 1
Properties used for the buried cast iron and PVC water pipes.

Properties	Cast iron	PVC	Soil A	Soil B	Water
a (m)	0.08	0.08	–	–	–
h (m)	0.01	0.01	–	–	–
Density (kg/m^3)	7100	2000	2000	2000	1000
Young's modulus (N/m^2)	1e11	5.0e9	–	–	–
Bulk's modulus (N/m^2)	–	–	5.3e7	4.5e9	2.25e9
Shear modulus (N/m^2)	–	–	2e7	1.8e8	–
Poisson's ratio	0.29	0.4	–	–	–
Material loss factor	0.001	0.065	–	–	–

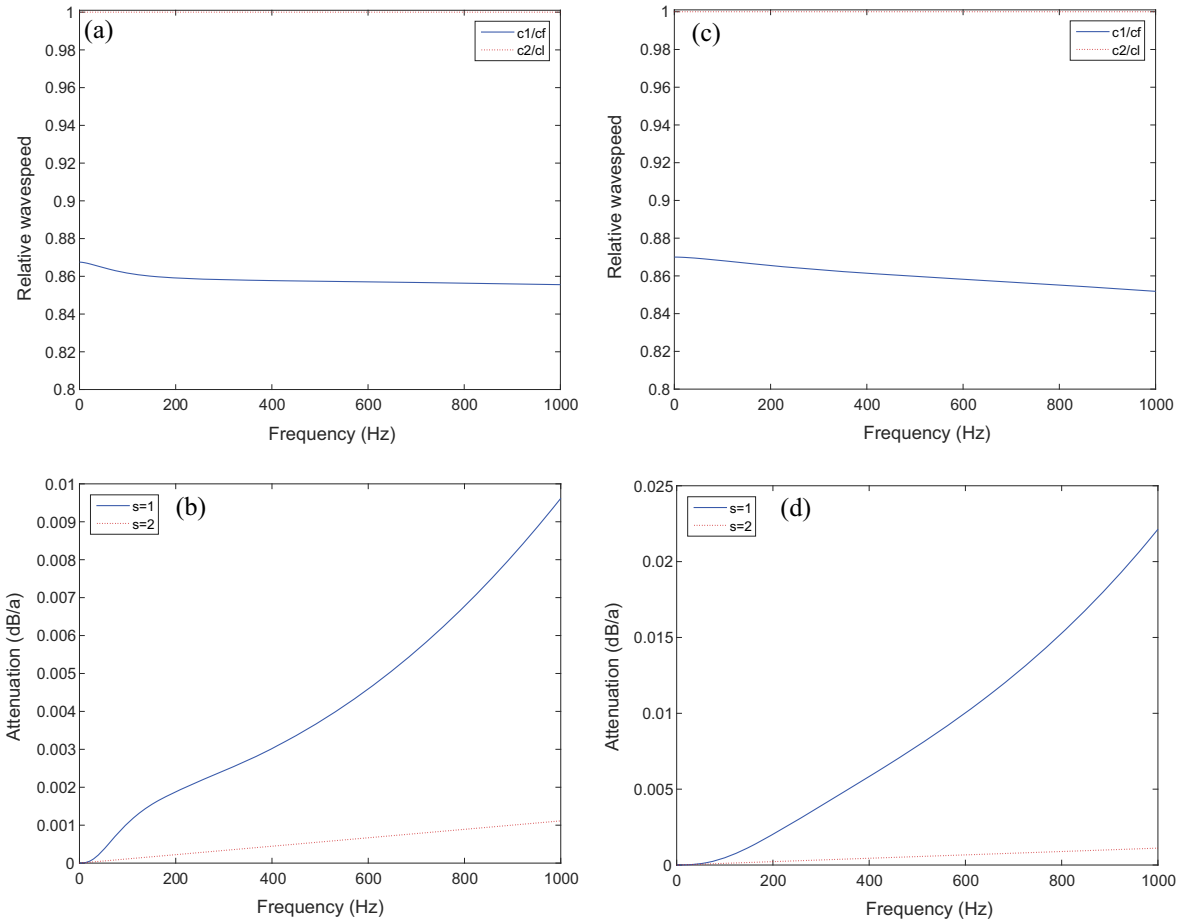

Fig. 2. Dispersion curves for the $s = 1, 2$ waves in a cast iron water pipe buried in sandy soil (A): (a) relative wavespeed; (b) attenuation (dB/a); and buried in clay soil (B): (c) relative wavespeed; (d) attenuation (dB/a).

4.1. The s = 1, 2 wave motions

For the cast iron pipe considered, the fluid loading is light, $Re(\beta) = 0.33$. As a result, the calculated wavespeed, c_1, is slightly less than the free-field fluid wavespeed, c_f, $c_1 = 0.86c_f$ for both soil types, as shown in Fig. 2(a) and (c). The decrease in wavespeed is mainly caused by the fluid loading compared to the insignificant effect of soil loading for metal pipes, and it decreases further with increasing frequency as a result of the inertia effect of the pipe wall, which can be seen from Eq. (6). It is observed that the $s = 2$ wavespeed coincides with the shell compressional wavespeed, suggesting that the $s = 2$ wave is effectively uncoupled from the internal fluid and the surrounding soil. The attenuation characteristics of the two wave types are plotted in Fig. 2(b) and (d). As expected, there is a significant increase of the attenuation for the $s = 1$ wave due to the additional radiation losses, in particular, at higher frequencies compared to the attenuation for the *in vacuo* pipe that varies approximately linearly with frequency arising from the material losses within the pipe wall. In contrast, for the $s = 2$ wave, the attenuation varies approximately linearly with frequency for losses within the pipe wall dominate, since the $s = 2$ wave is effectively uncoupled from the surrounding soil. In addition, the attenuation levels for the $s = 1$ wave is much greater than for the $s = 2$ wave, in particular in clay soil (B).

Fig. 3(a) and (b) show the ratios of the radial displacements and internal pressures for two soil types respectively. It can be seen that, both $|W_2/W_1|$ and $|P_{f2}/P_{f1}|$ decrease with frequency with sandy soil (A) being more effective for attenuating the $s = 2$ wave compared to the $s = 1$ wave in particular at lower frequencies. For clay soil (B), both ratios of the radial displacements and internal pressures reduce from the order of 10^{-4} to 10^{-9}. This implies that the contributions of the $s = 2$ wave to both the radial pipe wall and fluid motions are insignificant within the entire low frequency range of interest.

A similar trend can be seen in the case when the PVC pipe is buried in the two soil types. Comparing Figs. 2 and 4, it is found that the propagation wavespeed c_1 is much less than the free-field fluid wavespeed, c_f, for the plastic pipe with heavy fluid loading, $Re(\beta) = 6$; the attenuation in the PVC pipe has great attenuation levels for the $s = 1$ wave, with both material losses within the pipe wall and radiation losses contributing. The ratios of the radial displacements and internal pressures for

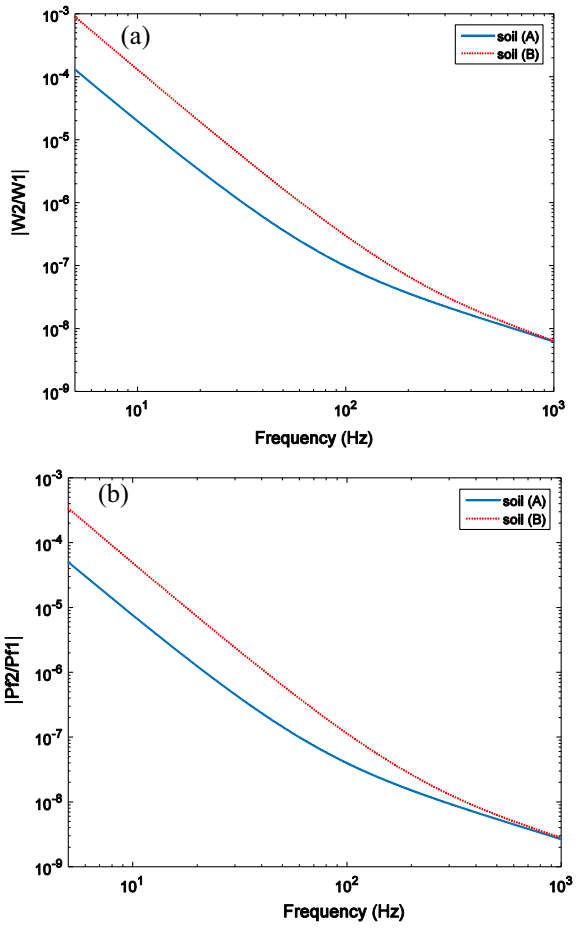

Fig. 3. Ratios of $s = 1$, 2 waves for a cast iron water pipe buried in two soils: (a) $|W_2/W_1|$; (b) $|P_{f2}/P_{f1}|$.

two soil types are plotted in Fig. 5(a) and (b) respectively. It can be seen that, for the clay soil, at lower frequencies below 10 Hz, $|W_2/W_1| = O(0.001)$ and $|P_{f2}/P_{f1}| = O(0.01)$; the radial displacement and pressure ratios drop significantly to 10^{-7} to 10^{-6} at 200 Hz. Despite slightly higher levels of the ratios obtained in the plastic pipe than in the metal pipe, the contributions of the $s = 2$ wave to the structural and fluid motions are still relatively small compared to the $s = 1$ wave.

In practical surveys using acoustic methods, the leak noise signals are dominated by ambient noise at very low frequencies. Therefore, as discussed above, the $s = 1$ wave is the propagating wave detected in water distribution pipes even though the $s = 2$ wave is excited.

4.2. Relationship between the radial pipe motion and the internal pressure

Upon adopting Eq. (11), it can be found that the radial pipe wall displacement is related to the internal pressure resulting from the $s = 1$ wave by χ_1. Substitution of k_1 given by Eq. (6) leads to

$$\left|\frac{W_1}{P_{f1}}\right| = \frac{a^2(1-\upsilon_p^2)/E_p h}{1-\Omega^2+\alpha} \tag{17}$$

Since hydrophones and accelerometers are typical leak detection sensors, by multiplying ω^2 in Eq. (17), the relationship between the acceleration response of the pipe wall and the pressure response is now obtained. Numerical results are plotted in Figs. 6(a) and (b) for the cast iron pipe and Figs. 6(c) and (d) for the PVC pipe respectively. As can be seen from Figs. 6 (a) and (c), the magnitudes of the ratio increase with frequency for both cast iron and PVC pipes. A slightly larger value is achieved for sandy soil (A) compared to clay soil (B) for the PVC pipe whereas the ratios are almost the same for the cast iron pipe buried in two types of soils. Thus the response of the pipe wall is much less compared to that within the contained fluid for buried water pipes. These ratios are found to be considerably small regardless of the pipe properties. This explains that, leak signals measured by hydrophones lead to significantly higher levels than by accelerometers. Comparing Figs. 6(b) and (d), it can be seen that strictly speaking, the pipe wall responses for both cast iron and PVC pipes are not in

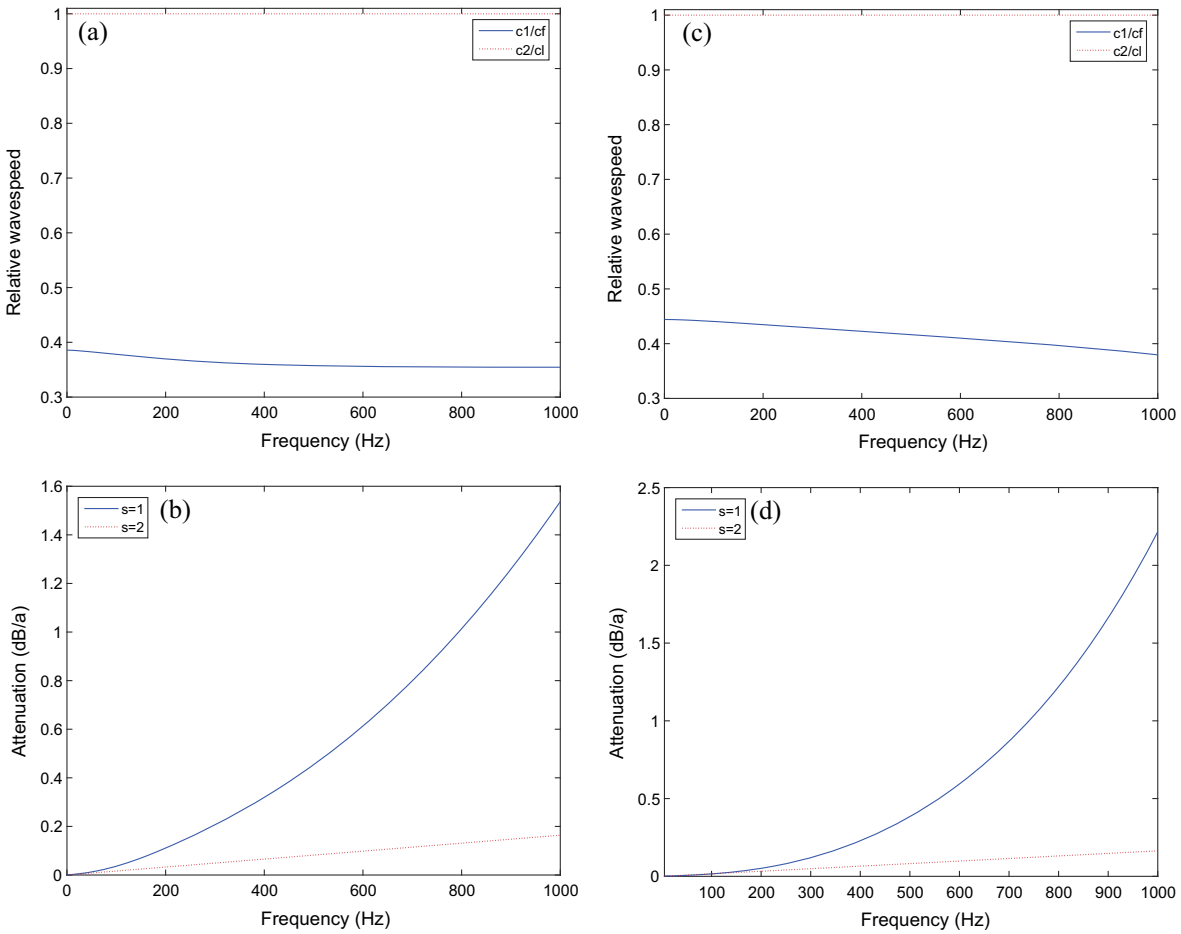

Fig. 4. Dispersion curves for the $s = 1, 2$ waves in a PVC water pipe buried in sandy soil (A): (a) relative wavespeed; (b) attenuation (dB/a); and buried in clay soil (B): (c) relative wavespeed; (d) attenuation (dB/a).

phase with the fluid response. However, noting that the most leak signals concentrate at the frequencies up to 1 kHz for metal pipes and 200 Hz for plastic pipes, the phase difference (being less than 0.05 for the cast iron pipe and 0.15 for the PVC pipe) are relatively small in these frequency ranges. Hence, the phase distortion between the radial pipe wall motion and fluid motion can be neglected at lower frequencies. Since the time difference in arrival leak signals is directly related to the phase information, both acoustic/vibration sensor can be employed to measure the propagating $s = 1$ wave such that almost identical results of phase information are provided for the determination of the leak position using acoustic cross-correlation methods.

5. Experiments and discussions

In this section, experimental results from two buried pipe systems are discussed, including a leak detection facility located at a National Research Council (NRC) site in Canada [10,11] and a buried MDPE pipe facility at the UEA in the UK [28]. Different excitation mechanisms were adopted for comparison: for the NRC test, measurements were carried out when water leakage occurred; for the UEA test, pressure measurements involved direct excitation of the fluid and the pipe fitting (hydrant).

5.1. Pressure response vs acceleration response

Leak detection tests were carried out at a NRC site. The descriptions of the NRC site and measurement procedures are detailed in [10,11]. The facility consisted of a 200 m length, 150 mm OD, PVC pipe buried in soft silty clay at a depth of 2.4 m. Several connection leaks, a joint leak and a crack leak were simulated on the test pipe. Here a joint leak was chosen and measured using hydrophones and accelerometers, as illustrated in Fig. 7. The pipe pressure throughout the tests were

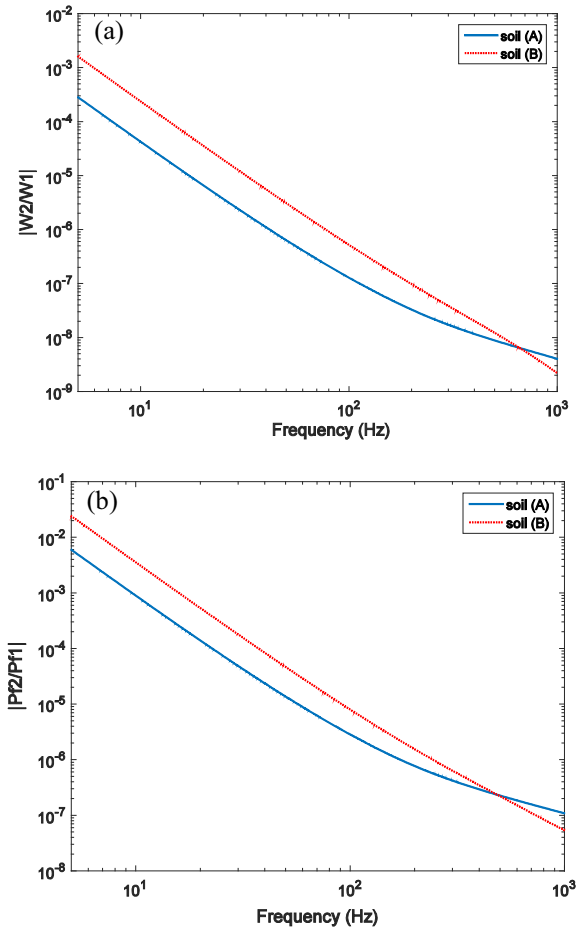

Fig. 5. Ratios of $s = 1$, 2 waves for a PVC water pipe buried in two soils: (a) $|W_2/W_1|$; (b) $|P_{f2}/P_{f1}|$.

345 kPa (50 psi) at various flow rates. Previous work has shown that for a particular pressure, the flow rate only affected the levels of the measured signals in the time domain, whereas the frequency contents remain unchanged [10].

The accelerometers were attached magnetically to the top surface of the fire hydrants while the hydrophones were pressurised with water. For acceleration measurement, piezoelectric accelerometers having a sensitivity of 1 V/g were used. For pressure measurement, hydrophones having a sensitivity of 44.7 V/bar were attached to fire hydrants through a special pipe fitting. The signals were each passed through an anti-aliasing filter with the cut-off frequency set at 200 Hz. Hydrophone-measured signals of 66-s duration were then digitised at a sampling frequency of 500 samples/s. The same sampling frequency was applied to the accelerometer-measured signals for a duration of 60 s.

Previous work on the correlation measurements [12–14] has shown that the water leak can be successfully detected at a range of 100 m. In the analysis, the $s = 1$ wavespeed was determined from the phase spectrum of two sensor signals, confirming that leak noise propagates as the $s = 1$ wave. Specifically, it has been shown in [12] that in the noise-free case, good levels of cross-correlation (and hence the accuracy of the leak location) are possible for ratios of sensor distances from the leak of less than about 10 (or greater than 0.1) for pressure responses and less than about 3 (or greater than 1/3) for acceleration responses. In the test, the distance between the two sensor locations was 102.6 m. This suggests that accurate leak detection can be achieved by measuring the pressure at two locations at the distances of 10–93 m or acceleration of 26–77 m from the leak source.

The aim of this section is to exploit the pressure and acceleration responses at a single location in order to better understand the acoustic/vibration signals for the detection of water leaks. Comparison of the pressure and acceleration responses is now made at the distance of 29.1 m from the leak source. Fig. 8 plots the time series of the measured signals in comparison with ambient noise (in the case of no leaks). It is apparent that the pressure responses have much higher levels than acceleration responses. This is also clearly shown in the frequency domain analysis, as plotted in Figs. 9(a) and (b). It can be seen from these figures that the hydrophone-measured leak signal has a much higher signal-to-noise ratio (SNR) than accelerometer-measured data below 100 Hz (in particular below 50 Hz) where most of the frequency content of leak signals is concentrated. In addition, the leak signal measured by the accelerometer is not significantly higher than ambient noise.

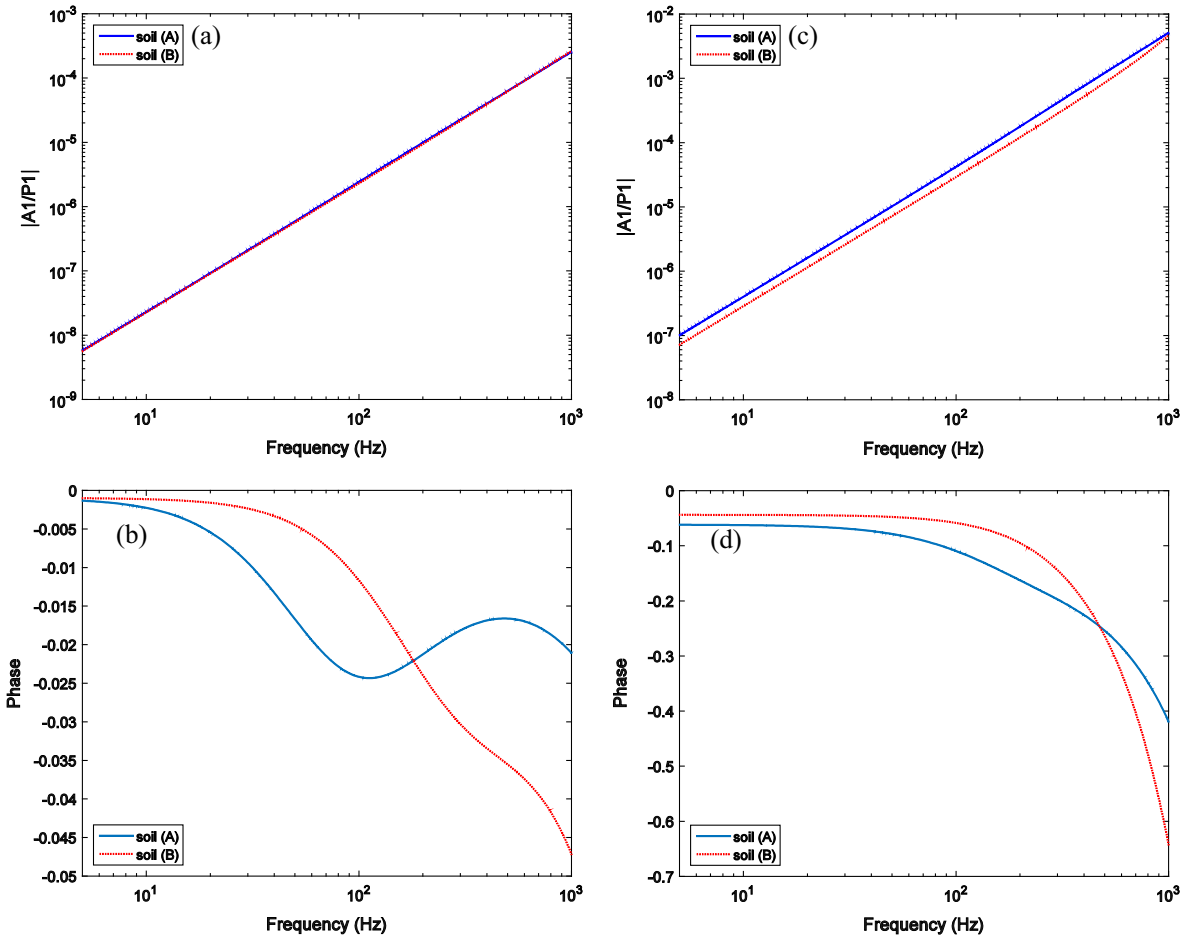

Fig. 6. Ratios of the acceleration response of the pipe wall and the pressure response for the $s = 1$ wave in a cast iron water pipe: (a) magnitude; (b) phase in radians; and in a PVC water pipe: (c) magnitude; (d) phase in radians.

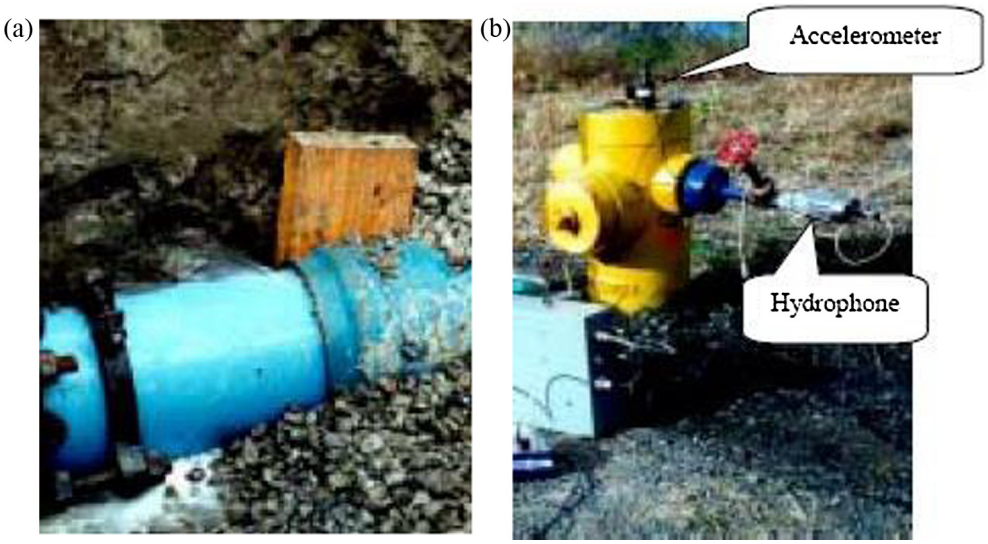

Fig. 7. Test site at the UEA: (a) a joint leak; (b) sensor attachment [10].

Thus, it explains that a measure of pressure response would be better suitable for locating leaks having small SNR, since the acceleration responses are easily corrupted by the existence of ambient noise.

5.2. Pipe excitation

Fig. 10 shows a schematic of the test rig at the UEA site constructed in an acoustically quiet environment, operating at a low pressure. The test rig comprised a 34 m length, 180 mm OD, MDPE pipe buried at a depth of approximately 1 m in loose, sandy soil. As illustrated in Fig. 11, pipe excitation measurements were conducted by using a sounder and an internal shaker driven by continuous random signals: a sounder (i.e., a modified moving-coil underwater loudspeaker) was installed in the pipe fittings and located at the end of the pipe; an inertial shaker was attached to the hydrant on the pipe. Each of the 4 m lengths were fitted with two hydrophones installed through the pipe wall such that the active face of the sensor was flushed with the inside bore of the pipe. The time domain signals of about 60 s were acquired from two pairs of hydrophones using the data capture software, DATS. Referring to Fig. 10, four hydrophones were, therefore, used in each measurement: H1–H4 acquired data from 4 m length – T (with a hydrant) – 4 m length; H5–H8 acquired data from 4 m length – T (with a gate vale) – 4 m length; H9–H12 acquired data from 4 m length – T (with a gate vale) – 4 m length. The sampling rate was 2000 samples/s. Spectral analysis was performed on the sensor signals using a 1024-points FFT, Hanning window (with 50% overlap), and power spectrum averaging. Hydrophone-measured signals H5–H8 were used in the analysis. The distance from H5 to the sounder was 11.39 m and the relative distances of H6–H8 from H5 were 2.05 m, 5.38 m, and 7.41 m respectively.

When the sounder were excited, the ASDs of H5–H8 and phase spectra relative to H5 are plotted in Figs. 12(a) and (b) respectively. It is noted that the sounder has a low frequency limit at which measurements can be made of approximately 30 Hz. As can be seen from the ASD plots, most of the frequency content of the propagating signals is concentrated in the frequency range up to 450 Hz, with the "noise floor" being reached at a lower frequency for the hydrophones further from the sounder. In addition, it is demonstrated that the pressure signals decay as they propagate away from the sounder. The peaks seen in the ASDs are harmonics of 50 Hz, which are likely due to the electronic interference. Examination of the phase

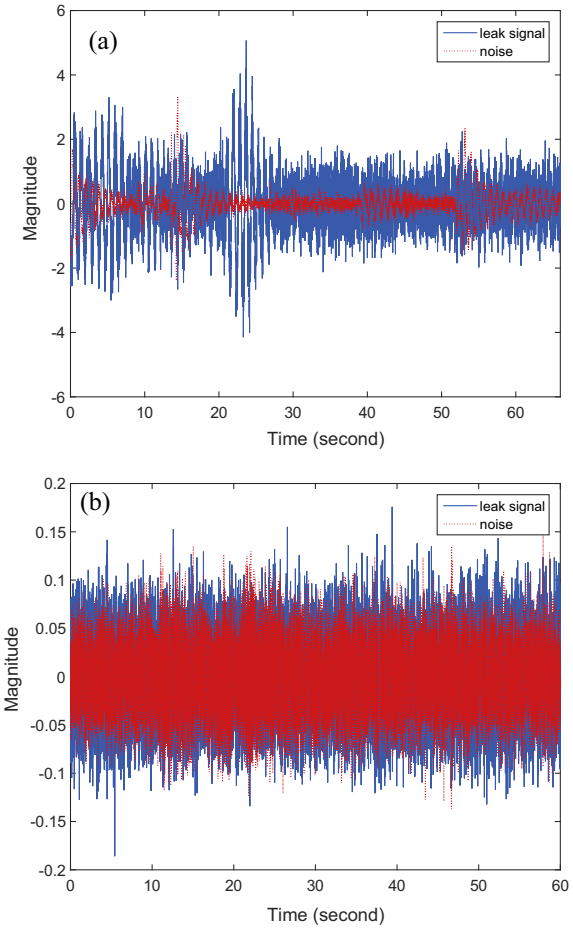

Fig. 8. Comparison of the signals measured by: (a) hydrophone and (b) accelerometer.

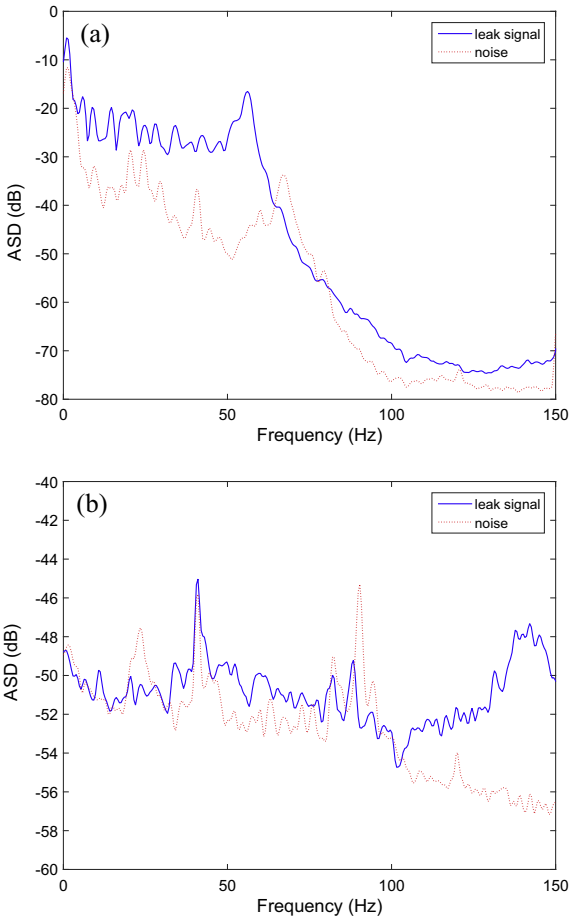

Fig. 9. Comparison of the ASDs of the signals measured by: (a) hydrophone and (b) accelerometer.

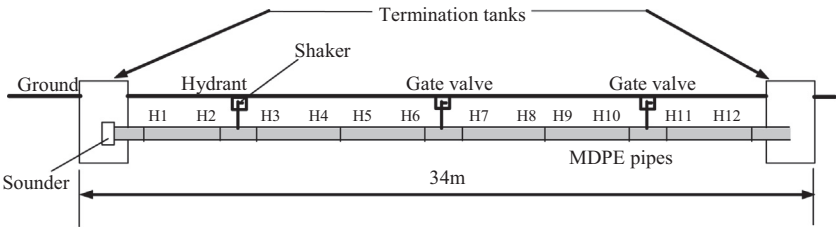

Fig. 10. Schematic of the test rig at the UEA [28].

spectra plotted in Figs. 12(b) shows the wavespeed is approximately 370–380 m/s, which is consistent with the wavenumber measurements of the $s = 1$ wave captured from the hydrophone pair nearest the sounder, H1 and H2, as reported in previous work by Muggleton et al. [26].

For the next set of experiments the pipe was excited using an inertial shaker attached to the hydrant on the pipe. The ASDs of H5–H8 and phase spectra of the hydrophones H6–H8 relative to H5 are plotted in Figs. 13(a) and (b) respectively. Compared to the excitation of the sounder, Figs. 12 and 13 illustrate very similar low-frequency behaviour of the ASDs and phase spectra of the hydrophone-measured signals. As expected, Fig. 13(a) clearly shows the presence of a propagating wave from H5 towards H8 (away from the shaker). When the shaker was driven by the continuous random signal, the wavespeed was found to be consistent with that derived from the measurements made with the sounder.

Test results confirm that the $s = 1$ wave propagates in the buried plastic pipe as a result of excitation of the fluid or the pipe fitting. When the shaker was in direct contact with the ground, however, no such wave was detected.

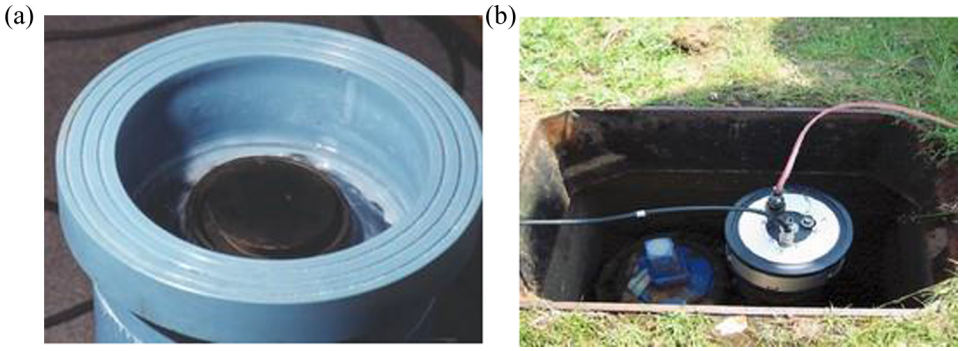

Fig. 11. Excitation of the pipe rig by using: (a) a sounder mounted in a flanged pipe fitting and (b) an inertial shaker mounted on the hydrant.

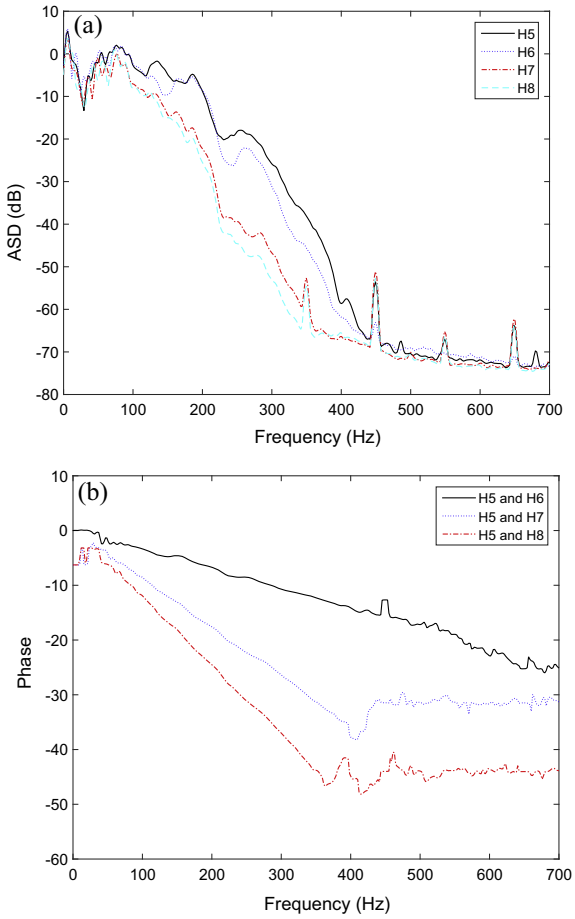

Fig. 12. The ASDs and phase spectra of hydrophone-measured signals when the sounder was excited: (a) ASDs of H5–H8 and (b) phase in radians.

6. Conclusions

Axisymmetric waves that propagate at low frequencies are of practical interest in the application of acoustic techniques for leak detection in water distribution pipes. The contributions made by the $n = 0$, $s = 1, 2$ waves to the structural and fluid motions have been investigated. Based on the coupled equations of motion for the $n = 0$ waves, analytical solutions to the two wavenumbers have been presented and the ratios of pipe wall motion and fluid motion have been derived for the buried fluid-filled pipe.

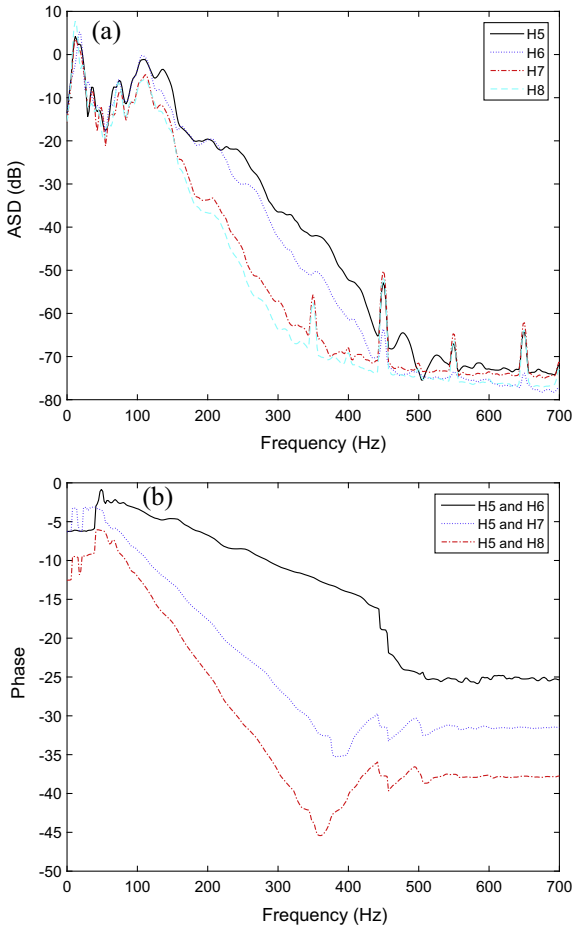

Fig. 13. The ASDs and phase spectra of hydrophone-measured signals when the pipe was excited using an inertial shaker: (a) ASDs of H5–H8 and (b) phase in radians.

Numerical analysis has been performed on a cast iron water pipe and a PVC water pipe. It has been found that for both pipes, the contributions of the $s = 2$ wave to both the pipe wall motion and fluid motion are negligible. This demonstrates that the $s = 1$ wave is responsible for the propagation of leak noise in buried water distribution pipes, which can be effectively detected by acoustic/vibration sensors in practical leak detection. Since pressure signals are less affected by ambient noise, they are better suited to detect water leaks in a low SNR environment. It has also been shown that the radial pipe wall motion can be evaluated by monitoring the internal pressure in response to the $s = 1$ wave (or vice versa).

Two buried pipe systems have been presented to support the theoretical findings. Leak signals from the NRC site have clearly shown that pressure response has a much higher SNR than acceleration response. Moreover, measurements at both sites have confirmed the $s = 1$ wave propagates at low frequencies in water distribution pipes as a result of water leakage and direct pipe excitation.

Acknowledgements

This work is funded by the CAS Hundred Talents Programme of China. The authors would like to thank the National Research Council of Canada and the EPSRC (under Grant GR/R13937/01) for providing the test data. Many thanks are also due to Professor Michael Brennan and Dr. Jennifer Muggleton for helpful discussions.

Appendix A. Supplementary material

Supplementary data associated with this article can be found, in the online version, at http://dx.doi.org/10.1016/j.ymssp.2016.12.018.

References

[1] United States Environmental Protection Agency, Control and Mitigation of Drinking Water Losses in Distribution Systems, EPA 816-R-10-019, Download from <www3.epa.gov>, 2010 (accessed June 2016).
[2] BDEW - German Association of Energy and Water Industries, VEWA Survey: Comparison of European Water and Waste water Prices, Download from <www.bdew.de>, 2010 (accessed June 2016).
[3] Y. Zhou, S.J. Jin, H. Feng, Z. Zeng, Z. Qu, Study on oil and gas pipeline leakage real-time in section system based on distributed optical fiber, Key Eng. Mater. 381 (2008) 447–450.
[4] A.F. Colombo, P. Lee, B.W. Karney, A selective literature review of transient-based leak detection methods, J. Hydroenvir. Res. 2 (4) (2009) 212–227.
[5] P.S. Murvay, I. Silea, A survey on gas leak detection and localization techniques, J. Loss Prevent. Proc. 25 (6) (2012) 966–973.
[6] L. Sun, Mathematical modeling of the flow in a pipeline with a leak, Math. Comput. Simulat. 82 (2012) 2253–2267.
[7] S. Demirci, E. Yigit, I.H. Eskidemir, C. Ozdemir, Ground penetrating radar imaging of water leaks from buried pipes based on back-projection method, NDT&E Int. 47 (2012) 35–42.
[8] H.V. Fuchs, R. Riehle, Ten years of experience with leak detection by acoustic signal analysis, Appl. Acoust. 33 (1991) 1–19.
[9] D.A. Liston, J.D. Liston, Leak detection techniques, J. New England Water Works Assoc. 106 (1992) 103–108.
[10] O. Hunaidi, W.T. Chu, Acoustical characteristics of leak signals in plastic water distribution pipes, Appl. Acoust. 58 (1999) 235–254.
[11] O. Hunaidi, W. Chu, A. Wang, W. Guan, Detecting leaks in plastic pipes, J. Am. Water Works Assoc. 92 (2000) 82–94.
[12] Y. Gao, M.J. Brennan, P.F. Joseph, J.M. Muggleton, O. Hunaidi, A model of the correlation function of leak noise in buried plastic pipes, J. Sound Vib. 277 (2004) 133–148.
[13] Y. Gao, M.J. Brennan, P.F. Joseph, J.M. Muggleton, O. Hunaidi, On the selection of acoustic/vibration sensors for leak detection in plastic water pipes, J. Sound Vib. 283 (3–5) (2005) 927–941.
[14] Y. Gao, M.J. Brennan, P.F. Joseph, A comparison of time delay estimators for the detection of leak noise signals in plastic water distribution pipes, J. Sound Vib. 292 (2006) 552–570.
[15] O. Hunaidi, A. Wang, A new system for locating leaks in urban water distribution pipes, J. Environ. Qual. 7 (4) (2006) 450–466.
[16] Y.A. Khulief, A. Khalifa, R.B. Mansour, M.A. Habib, Acoustic detection of leaks in water pipelines using measurements inside pipe, J Pipeline Syst. Eng. 3 (2) (2012) 47–54.
[17] A.J. Brunner, M. Barbezat, Acoustic emission monitoring of leaks in pipes for transport of liquid and gaseous media: a model experiment, Adv. Mater. Res. 13–14 (2006) 351–356.
[18] A. Anastasopoulos, D. Kourousis, K. Bollas, Acoustic emission leak detection of liquid filled buried pipeline, J. Acoustic Emission 27 (2009) 27–39.
[19] M.F. Ghazali, S.B.M. Beck, J.D. Shucksmith, J.B. Boxall, W.J. Staszewski, Comparative study of instantaneous frequency based methods for leak detection in pipeline networks, Mech. Syst. Signal Process. 29 (2012) 187–200.
[20] N. Metje, P.R. Atkins, M.J. Brennan, D.N. Chapman, H.M. Lim, J. Machell, J.M. Muggleton, S. Pennock, J. Ratcliffe, M. Redfern, C.D.F. Rogers, A.J. Saul, Q. Shan, S. Swingler, A.M. Thomas, Mapping the underworld – state-of-the-art review, Undergr. Sp. Tech. 22 (2007) 568–586.
[21] C.R. Fuller, F.J. Fahy, Characteristics of wave-propagation and energy-distributions in cylindrical elastic shells filled with fluid, J. Sound Vib. 81 (1982) 501–518.
[22] C.R. Fuller, The input mobility of an infinite circular cylindrical elastic shell filled with fluid, J. Sound Vib. 87 (1983) 409–427.
[23] R.J. Pinnington, A.R. Briscoe, Externally applied sensor for axisymmetrical waves in a fluid-filled pipe, J. Sound Vib. 173 (1994) 503–516.
[24] J.M. Muggleton, J. Yan, Wavenumber prediction and measurement of axisymmetric waves in buried fluid-filled pipes: inclusion of shear coupling at a lubricated pipe/soil interface, J. Sound Vib. 332 (2013) 1216–1230.
[25] Y. Gao, F. Sui, J.M. Muggleton, J. Yang, Simplified dispersion relationships for fluid-dominated axisymmetric wave motion in buried fluid-filled pipes, J. Sound Vib. 375 (2016) 386–402.
[26] J.M. Muggleton, M.J. Brennan, P.W. Linford, Axisymmetric wave propagation in fluid-filled pipes: wavenumber measurements in in vacuo and buried pipes, J. Sound Vib. 270 (2004) 171–190.
[27] M. Abramowitz, I.A. Stegun, Handbook of Mathematical Functions, Dover publications, INC., New York, 1970 (Chapter 9).
[28] Y. Gao, Leak detection in plastic water pipes PhD Thesis, Institute of Sound and Vibration Research, University of Southampton, UK, 2006.